THE EFFECT OF RIM ANGLE ON PARABOLIC DISHES FOR HIGH THERMAL PERFORMANCE AND RADIATION CONCENTRATION

Raaid Allam

Bachelor of Engineering
Major in Mechanical Engineering

Department of Mechanical Engineering
Macquarie University

November 12, 2017

Supervisor: Dr Yijiao Jiang
Co-Supervisor: Dr Sicong Tian

Acknowledgements

I would like to say thank you to my supervisor Dr. Yijiao Jiang for allowing me to be part of this research. I would like to thank Dr. Sicong Tian for the advice and support during the course of this research.

I want to express my sincere gratitude to my family, especially my mother Fatme Ghamloush for the everlasting support and encouragement. Thank you for being a part of my journey, without you I wouldn't have achieved this today.

Statement of Candidate

I, Raaid Allam, declare that this report, submitted as part of the requirement for the award of Bachelor of Engineering (Honours) in the Department of Mechanical University, Macquarie University, is entirely my own work unless otherwise referenced or acknowledged. This document has not been submitted for qualification or assessment at any other academic institution.

Student's Name: Raaid Allam

Student's Signature: Raaid Allam

Date: 12 November, 2017

Abstract

In this research concentrated solar power (CSP) technologies have been studied. The history of solar concentration deployment and commissioning have been mentioned. Solar parabolic concentrators have been chosen as the main field of the research. Therefore determining the rim angle is an important factor when developing solar parabolic dishes. A testing rig was developed to investigated the effects of three rim angles (30°, 45° & 60°) on the concentration ratio and thermal performance of the system. A solar simulator was used to test the dishes which emits rays having the same quality of the sun. It was determined the 60° rim angle can provide the highest concentration ratio and thermal performance, although the efficiencies of the system for other angles are more stable.

Table of Contents

List of Figures

List of Tables

List of Abbreviations

CSP – Concentrated solar power

DNI – Direct normal irradiance

A_{con} – Area of concentrator aperture (m^2)

A_{dish} – Surface area of dish (m^2)

A_{rec} – Area of receiving region (m^2)

C_{max} – Maximum concentration ratio

$C_{con,\ max}$ – Highest obtainable concentration ratio.

D_{con} – Diameter of concentrator (m)

D_{rec} – Diameter of receiver (m)

$D_{rec,\ max}$ – Maximum achievable diameter receiver (m)

f – Focal length (m)

I – Solar irradiance (W/m^2)

h – Height of the dish (m)

K – Constant

Q_p – Density power output of simulator (W/m^2)

Q_{rad} – Radiative heat transfer (W)

$Q_{rad,\ incident}$ – Radiative heat transfer of incident transfer (W/m^2)

$Q_{rad,\ rec}$ – Radiative transfer to receiver (W/m^2)

$Q_{rad,\ solar\ simulator}$ – Radiative transfer of solar simulator (W/m^2)

R_{rad} – Radiative transfer ratio

T_{max} – Maximum concentrated temperature (°C)

T_{min} – Ambient temperature of receiver (°C)

$\alpha_{Qrad,\ eff}$ – Radiative heat transfer efficiency

ε – Emissivity of Material

σ – Stephan Boltzman constant

ρ – Reflectivity of material

δ – Absorptivity of material

θ_{acc} – Acceptance angle (deg)

θ_{rim} – Rim angle (deg)

Θ_s – Angle subtended by the sun (deg)

CHAPTER 1

1 Introduction

Our planet is privileged with a rich source of solar energy capable of providing 885 million terawatts hour to the earth's surface every year. This total is equivalent to 6,200 times the overall energy consumed by humans in 2008. In clear conditions, the sun can provide 1 kW/m² of solar radiation to the earth's surface which is the direct normal irradiance (DNI). This is an important parameter when considering surfaces such as mirrors and lenses for power generation purposes. This parameter measures the amount of energy received by the surface in kW/m² when it is perpendicular to sun rays. High DNI is available in regions such as North Africa, southern Africa, north-western India, the Middle East, northern Mexico, south-western United States, Australia, Peru and Chile. Parts of these regions have the essential requirements for receiving high DNI, which are hot and dry climates and geomorphological elevation [1, 2].

The main contribution for global warming is the burning of fossil fuels, coal and natural gas for power generationa and transport. A solution proposed for eliminating the risk of climate change is to transition for fossil fuel to non-fossil fuel energy. Many countries have taken the initiave for the development of concentrated solar power plants such as Spain and the US, but many others are following such as China, Morocco and Sweden. The route to complete transition is still too long since renewable energy power generation was responsible for 28 % of all global consumption exceeding 1,811 GW in 2015. Only 12 % of the total generated renewable energy was via the utilization of solar power. Although it seems a long route but progress has been noticed since in 2015, the newly installed power generating technologies that were based on renewable energy exceeded those based on fossil fuels and other pollutants [3].

Generating electricity by renewable energy routes will reduce carbon emissions drastically from fossil fuels, coal and other conventional air pollutants. In 2008, 47.3 billion kWh of electricity was generated by renewable energy which reduced carbon emissions by 40 million metric tons during that year. Investment in the energy section reached 1.8

million US dollars in 2015 and more than half of this amount has invested in the oil, coal and gas sector. Therefore to be able to give up on polluting energies, research and development is committed to improve the solar thermal electricity generation sector. This can be done by improving the efficiency of solar plants and reducing operation and deployment costs [4, 5].

1.1 Motivation Behind Research

Even though it is hard to believe but more than one billion people remain in the dark without the access to electricity. Also, more than 3 billion use traditional sources of energy for cooking and heating. Solar energy can be used as a sustainable source of energy for electricity generation for lacking populations [3]. It is estimated that 17% of the world population do not have electricity and 95% of those are living in rural areas located in sub-Saharan Africa and Asia [1, 2]. Rural locations in India such as Rajasthan, Gujarat, Madhya Pradesh, Jammu and Kashmir are blessed with annual direct normal incidence of 1800 kWh/m^2 which makes them suitable candidates for CSP plant applications [6]. Chinese rural areas can benefit from CSP technologies since they have a high annual DNI. Rural areas in Tibet, Gansu, Xinjiang and Yunan receive Direct normal incidence above 3.2 kWh/(m^2 day) which is more than enough for CSP plant deployment [7]. Sub-Saharan Africa is the area with the least electricity in the world. Poor residents live in rural settlements in the dark because conventional grid electricity is very expensive to deploy. The dispersion of settlements is a main problem, therefore small scale CSP technologies could be the solution [8]. Rural Australia is a good candidate for CSP plants especially parabolic dish systems. Although electricity is available in Australia to everyone but it receives an approximate annual DNI of 2000 kWh/m^2, which is a suitable requirement of deploying CSP systems. Also, these systems require large landscapes to be deployed which are also available across the country. The scarcity of water is a major disadvantage for some CSP technologies such as Linear Fresnel, parabolic trough and central receiver systems which is needed for cooling purposes. This requirement is not needed for parabolic dish systems since water is only needed for mirror cleaning purposes [9].

1.2 Project Scope

The scope of this research is to study solar concentrated solar power systems, specifically solar parabolic concentrators, and provide a concept to achieve higher thermal radiation concentration which will lead to higher working temperatures. This research will study the effects of different rim angles on the concentration ratio and efficiency of a solar parabolic system.

1.3 Project Plan

Intensive research has been made in the field of solar energy and concentrated solar power technologies. A concenpt has been proposed to developed a portable concentrated solar parabolic dish with thermal storage capacity that will provide electricity over the hour for rural areas. It is known that thermal storage can be achieved through thermochemical processes such as methane reforming which requires elevated temperatures [10]. Therefore the effect of the rim angle on the parabolic concentrated has been taken as the study subject. Several literatures have been searched regarding the effects of the rim angle. Most of these literatures discussed results based on simulations, therefore small parabolic dish models were developed and tested. Each dish was designed to have the same diameter (300 mm) but different rim angle (30°, 45° & 60°). A testing rig was developed to test each dish using a solar simulator at different power outputs. The efficiency, thermal performance and concentration ratio for each angle was determined and compared.

1.4 Project Budget

This project was funded by Macquarie university. A testing rig was designed and the materials required for assembly and development are listed in the *Table 1.1*.

Table 1.1 Material dimensions, quantity and cost.

Material	Dimensions	Quantity	Price ($)
Linear Bearings	Bore Diameter 20 mm	x 6	102
Timber	W:70 H:70 L:1800 mm	x 3	76.59
	W:42 H:42 L:1800 mm	x 1	11.87
Wood Panel	W:900 H:12 L:1200 mm	x 1	22.50
Aluminum Rod	O.D.: 20, L:6000 mm	x 1	40
Shaft support	Bore Diameter 20 mm	x 6	30
Fresnel Lens	Dia.: 317.5, FL: 584.2 mm	x 1	90
Concave Lens	Dia.: 79.4, FL: 97 mm	x 1	7.5
Total			$ 380.46

1.5 Thesis Overview

In chapter 2, the history and fundamentals of solar energy will be discussed. In addition to results obtained by other studies to determine the effect of the rim angle on a parabolic dish. In the following chapter, design and development of the testing rig will be illustrated. In chapter 4, experimental results will be discussed and compared to other results determined by other studies. In chapter 5 a final conclusion will be drawn from the discussed results. Finally chapeter 6 will discuss the future impact of this research on other studies.

CHAPTER 2

2 Background and Related Work

2.1 History of Solar Energy

In the 1970s the first efforts for solar thermal electricity technology research started. In the following decade, the first commercial solar parabolic trough system started operating and generating 14 MW. In the 1990s, nine solar energy generating systems were operating with a total capacity of 354 MW which includes two pilot molten salt solar tower systems. In 2004 the construction of the first pilot parabolic dish Stirling engine system started and capable of generating 150 kW. The first commercial solar tower system (PS10) was deployed in 2007 operating at 10 MW near Seville, in Andalusia Spain. During the same year Solar One (60 MW), a commercial parabolic trough system was deployed in Nevada USA. In 2008 the first linear Fresnel system was developed in Kimberlina US generating power at 15 KW. In this same year a 50 MW commercial solar power plant was commissioned and it was called Andasol I, in Andalusia Spain. In the following year Spain deployed PS20, a 20 MW solar tower system, and PE1, a 1.4 MW linear Fresnel system. The US deployed a 5 MW solar tower system called Seirra Sun Tower in the same year. In 2010, 12 additional 50 MW concentrated solar power plants were put in operation in Spain in addition to the deployment of a 5 MW commercial scale dish Stirling engine in Maricopa US [11].

The main contribution for global warming is the burning of fossil fuels, coal and natural gas. A solution proposed for eliminating the risk of climate change is to transition for fossil fuel to non-fossil fuel energy. Renewable energy power generation was responsible for 28 % of all global consumption exceeding 1,811 GW in 2015. Only 12 % of the total generated renewable energy was via the utilization of solar power. Installation of renewable energy technologies has exceeded non-renewable technologies for electricity generation in 2012. In 2015, the newly installed power generating technologies that were based on renewable energy exceeded those based on fossil fuels and other pollutants [3].

2.2 Concentrated Solar Power Collector Technologies

There are four types of solar concentrating technologies used currently in trial and commercial CSP plants which are linear Fresnel (FL), parabolic trough collectors (PT), central receiver systems (CR) and parabolic dish systems (PD) [12].

2.2.1 Parabolic Trough Systems

Parabolic trough systems consist of an array of parabolic mirrors that focus solar radiation along their focal line where an absorber tube is mounted. The mirrors and the tubes are integrated with a sun tracking system. The absorber tube either carries a heat transfer fluid (HTF) such as molten salt that will enter a heat exchanger or it will directly generate steam by using water or air as the transfer fluid in a process direct steam generation (DSG) [13]. These systems have a concentration factor between 30 and 80. Temperatures of the thermal fluid can reach up to 500 °C, allowing for thermal power outputs of 30 to 700 MW. These systems are suitable for power generation through Rankine cycles [12].

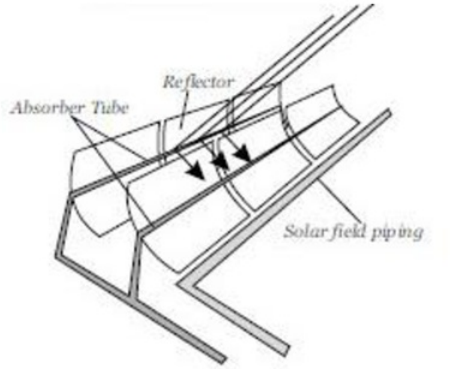

Figure 2.1 Parabolic trough technology [14].

2.2.2 Central Receiver Systems

Central receiver (CR) systems consist of a large field of reflectors called the heliostat field which focus solar radiation onto a receiver mounted on a central tower. In this system, the heliostat might be flat or slightly concave and are integrated with a sun tracking system. CR systems can achieve high temperatures and thus have high conversion

efficiencies. Both types of fluids can be used in CR systems, DSG and HTF [13]. The concentration factor that can be reached is between 200 and 1000. The temperature of the thermal fluid can exceed 500 °C, allowing for thermal power outputs of 50 to 300 MW. These systems are suitable for power generation through thermochemical processes or thermodynamic cycles [12].

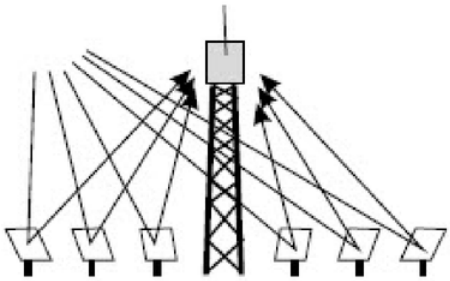

Figure 2.2 Central receiver technology [14].

2.2.3 Linear Fresnel Systems

Linear Fresnel systems have a similar mirror arraignment to parabolic trough systems but solar radiation is focused onto one focal line instead of a several. The mirrors are incorporated with a mirror tracking system that can follow the sun. Direct steam generation can be achieved in this system and thus disregarding the need of heat exchangers and heat transfer fluids. This system is less efficient than PT and CR systems and therefore cannot be integrated with thermal storage systems [13]. These systems are very similar to LF technologies in the sense of concentration factor and output power generation [12].

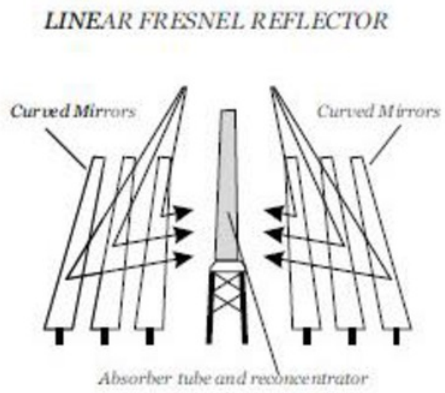

Figure 2.3 Linear Fresnel technology [14].

2.2.4 Parabolic Dish Systems

Parabolic dish systems concentrate solar radiation onto a small region called the focal area above the centre of the dish. The collector and the receiver are integrated with a solar tracking system which move together. These systems are able to achieve the highest transformation efficiency compared to any other CSP technology [13]. The concentration factor C ranges between 1000 and 3000 for this technology which have proven to have the highest efficiency than other CSP technology by an approximate conversion rate of 30% of DNI solar radiation into electricity while considering parasitic power losses [12, 15].

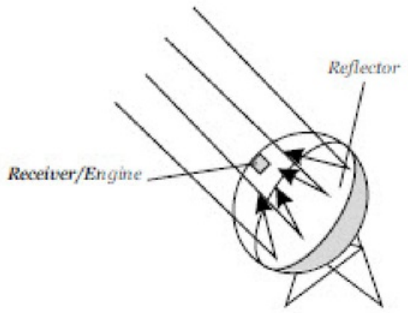

Figure 2.4 Parabolic dish technology [14]

2.3 Thermochemical Processes

Solar thermochemical processes convert solar radiation into chemical energy for storage and transport. The thermochemical process is dictated by the 1st and 2nd laws of thermodynamics. By applying the 1st law, the minimum amount of solar energy required to produce a specific amount of solar fuel can be determined. The 2nd law is applied to determine whether the chosen route to produce the fuel is physically feasible [16]. There are several types of solar thermochemical processes which are classified in *Figure 2.5* [17]. These processes are divided into hydrogen/sygnas production and industrial applications. Electricity production falls in the hydrogen/syngas production section, which can be achieved by solar thermolysis, hydrocarbon feed or thermochemical cycles sub processes [17]. But only some common processes will be discussed.

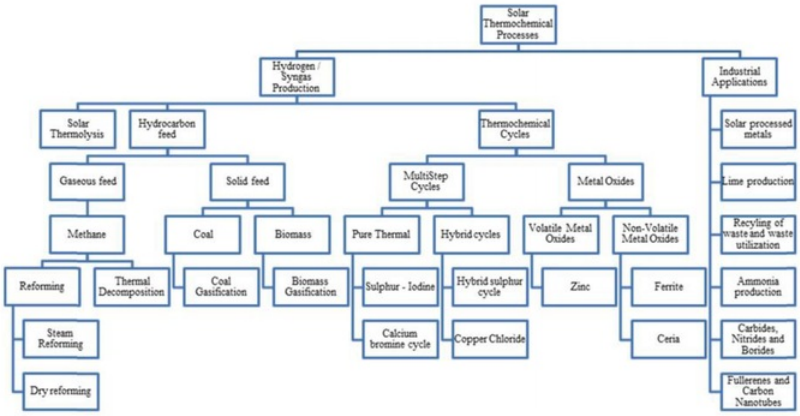

Figure 2.5 Thermochemical processes [17].

Solar thermolysis is a single step H_2O to H_2 conversion which can be specifically called, water thermolysis. The chemical reaction which describes this process is given by [18].

$$H_2O \rightarrow H_2 + 0.5O_2$$

This reaction includes a very high temperature requirement (above 2500 K) to achieve reasonable dissociation of water. An effective separation technique is also required to separate to products of the reaction to avoid having an explosive mixture [18]. Therefore, other

methods were introduced to avoid the high temperature requirement and separation problem.

The temperature requirements for thermochemical cycles and hydrocarbon feed processes are lower than for solar thermolysis and can be achieved by the available technology [17]. Solar reforming processes falls under the hydrocarbon feed processes and is a transformation that can utilize the thermal radiation collected from the sun to produce syngas (CO & H_2). The applications that will benefit from syngas synthesis can be finding an alternative for power production plants, hydrogen or methanol generation for transport applications, transforming biomass or organic waste into solar fuels. There are two types of solar reforming processes which are steam reforming and dry reforming. Methane dry reforming is when CO_2 is used as an oxidant as seen in reaction (1) below instead of steam for methane steam reforming as seen in reaction (2) below. Both types of reforming are highly endothermic processes that require a high amount of heat to trigger the chemical reaction. The favoured temperature range to trigger these chemical reactions is between $900\ ° - 1000\ °C$. The chemical reactions for both reforming processes are given by [10, 19].

$$CH_4 + H_2O \leftrightarrow 3H_2 + CO \qquad \Delta H = 205\,kJ/mol \qquad (1)$$
$$CH_4 + CO_2 \leftrightarrow 2H_2 + 2CO \qquad \Delta H = 246\ kJ/mol \qquad (2)$$
$$CO + H_2O \leftrightarrow H_2 + CO_2 \qquad \Delta H = -46\ kJ/mol \qquad (3)$$

Metal oxides redox reaction cycles are part of multi-step thermochemical cycles, which may be classified as volatile and non-volatile cycles. Cerium oxide is a non volatile metal oxide and can be used with H_2O and CO_2 in a 2-step thermochemical cycle to produce syngas via a redox reaction. The 2-step thermochemical process can be given by [17, 20].

$$High - T\ reduction: \qquad CeO_2 \overset{\Delta H}{\rightarrow} CeO_{2-\delta} + \frac{\delta}{2}O_2 \qquad (1)$$
$$Low - T\ oxidation\ with\ H_2O: \qquad CeO_{2-\delta} + \delta H_2O \rightarrow CeO_2 + \delta H_2 \qquad (2)$$
$$Low - T\ oxidation\ with\ CO_2: \qquad CeO_{2-\delta} + \delta CO_2 \rightarrow CeO_2 + \delta CO \qquad (3)$$

In the high temperature reduction step, cerium is reduced thermally to a non-stoichiometric state at a temperature above than 1673 K. In the low temperature oxidation step, ceria is oxidized with CO_2 or H_2O at a temperature lower than 1673 K [20]. Zinc redox reaction is another type of reaction used in thermochemical cycles, which is also a two-step cycle. In this case zinc oxide is an example of a volatile metal oxide. The first is reaction is highly endothermic and requires a temperature of 2235 K and second is an exothermic reaction which is favoured at a temperature below 1400 K. These reactions are given as [17].

$$High-T\ reduction: \quad ZnO \rightarrow Zn + \frac{1}{2}O_2 \qquad \Delta H = 478\,kJ/mol \qquad (1)$$

$$Low-T\ hydrolysis: \quad Zn + H_2O \rightarrow ZnO + H_2 \qquad \Delta H = -104\,kJ/mol \qquad (2)$$

2.4 Concentrated Solar Power Receiver Technologies

In this section several receiver/reactor designs will be discussed that can enable thermochemical processes.

Steinfeld, Brack, Meier, Weidenkaff and Wuillemin (1997), experimented on a solar reactor that will allow a non-volatile metal oxide thermochemical process, called Zinc oxide redox reaction. Symet, the name of reactor, which is a cavity type receiver and consists of an insulated cylindrical cavity containing a circular windowed aperture to allow the entering of concentrated solar radiation. The configuration of the receiver/reactor is shown in *Figure 2.6*. ZnO and CH_4 will flow into the reactor through a spiral groove around the reactor cavity as seen in *Figure 2.7*. The accumulation of heat inside the cavity will trigger the thermochemical process allowing for Zn and syngas (CO and H_2) to flow out of the receiver into a storage unit [21].

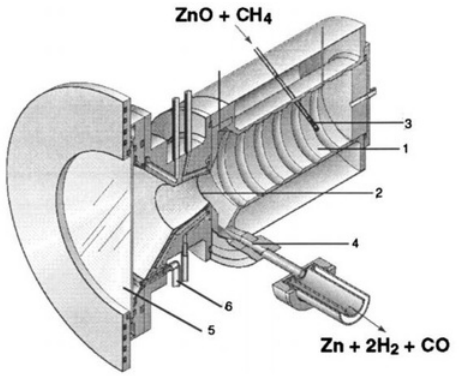

Figure 2.6 Zinc oxide thermochemical reactor model [21].

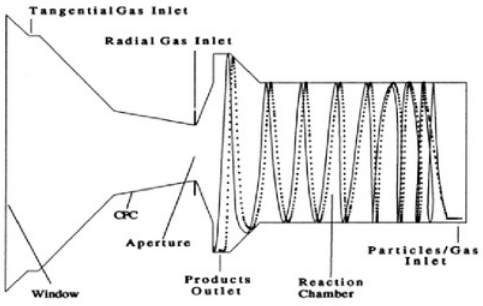

Figure 2.7 Zinc oxide thermochemical reactor sketch [21].

Buck, Muir and Hogan (1991), experimented with solar reforming of methane with CO_2 using a volumetric receiver reactor. Solar radiation will enter the receiver through an aperture. The reactor consists of an absorber that will have a major contribution to the chemical reaction. The absorber is made from porous ceramic material that will allow a uniform flow of the reactants. *Figure 2.8* shows the configuration of the reactor and the absorber within. CO_2 and CH_4 will enter the reactor through an inlet and will flow through the porous absorber. The temperature at the absorber will rise due to solar radiation, thus triggering a chemical reaction to produce H_2 and CO. Syngas will leave the reactor into a storage unit [22].

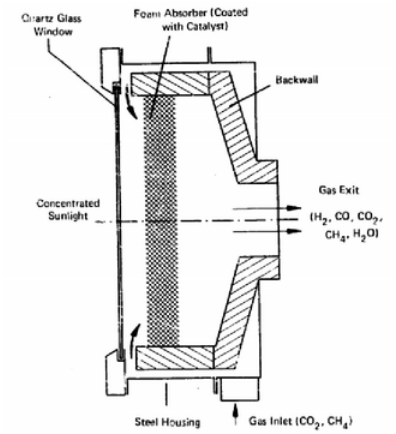

Figure 2.8 Thermochemical absorber [22].

2.5 Effects of Rim Angles on Solar Parabolic Dishes

Parabolic dish systems are the most efficient concentrated solar power technologies which can achieve a concentration ratio of 10,000 suns. The high concentration will enable high efficiencies and thus higher temperatures than other CSP technologies. This advantage will allow these systems to be used for multiple applications such as thermochemical storage systems and the production of solar fuels [23].

Sup, Zainudin, ZanariahShamsirAli, Bakar and Ming (2015) studied the image flux distribution of a solar parabolic dish at different rim angles. A 1 meter parabolic dish was simulated on Tonatiuh software and changes to the focal length have been made for each experiment. The parabolic dishes tested had focal lengths from 250 to 1500 mm in increments of 250 mm. The results are shown in the *Table 2.1* below. According to their work, the smaller the diameter of the image formed, a higher temperature can be achieved [24].

Table 2.1 Effects of rim angle on diameter of image [24].

focus point [mm]	θ rim ideal	diameter image [mm]	diameter non image [mm]	θ rim image	θ rim non image
250	180.00	8.00	22.04	180.00	180.00
500	106.26	6.60	12.80	105.90	105.55
750	73.74	13.60	22.80	100.20	99.72
1000	56.14	8.32	12.74	78.64	78.47
1250	45.24	4.00	12.60	64.52	64.21
1500	37.84	16.00	20.00	54.09	53.97

Wang and Siddique (2010) simulated a three-dimensional model of parabolic dish on the FEMAP software. The parabolic dish was designed based on the basic equation of a parabola with 1.68 m diameter and rim angles set to 30°, 45° and 60°. The results showed that the variation in rim angle had a negligible effect on the thermal performance of the receiver. However, these results were not conclusive since the thermal losses in the simulated receiver were very small. Wang and Siddique stated that ray tracing simulations were required to confirm the results [23]. Beltran, Velazquez, Espericueta, Sauceda and Perez (2012) performed a study on solar parabolic dishes using a mathematical model. One of the variables used in this model was the rim angle of the parabola. Their results are presented in the *Figure 2.9* below and which show that the highest concentration ratio is achieved at a rim angle of 45°regardless of the total geometric error of the concentrator. The reason behind that conclusion is that at a 45° rim angle the best comprise can occur between the width of the focal area and the distance between the focal region and the surface of the dish [25].

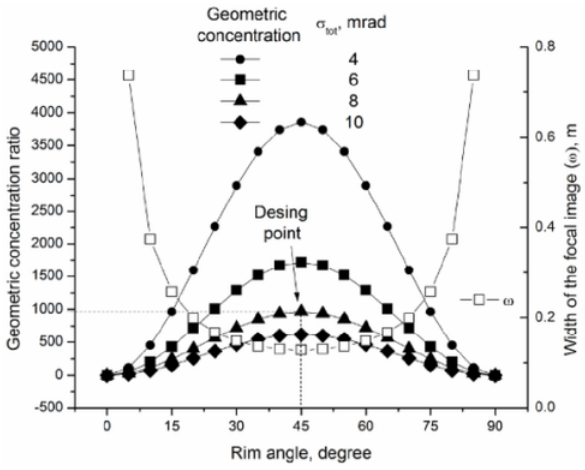

Figure 2.9 Effects of rim angle on geometric concentration [23].

Harris and Lenz (1983) analysed a model that would study the effects of the parabolic rim angle on the efficiency and power output of the system. They analysed 4 rim angles of values 45 to 75 in 10° increments. All angles had the same effect on system efficiency but the only change noticed was on the power profile of the receiver. This is evident in *Figure 2.10* below where the maximum radiant flux is almost the same for all rim angles but at different locations of the receiver. What can be taken from their research study is that different rim angle may achieve different power profiles on the absorber but it does not influence the overall efficiency of the system [26].

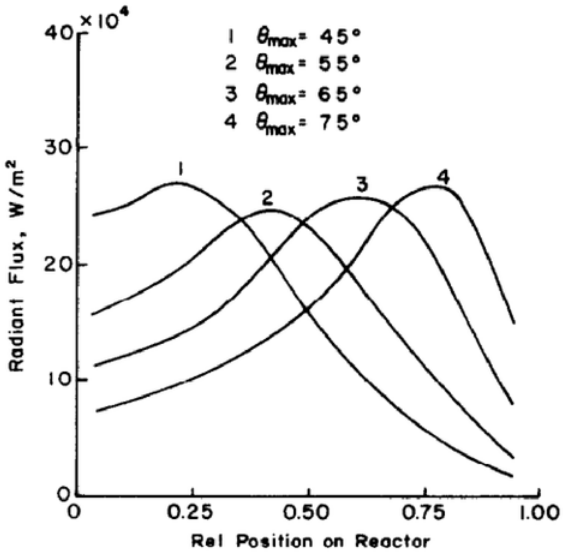

Figure 2.10 Effects of rim angle on radiation flux [26].

Many academics and researchers have discussed the advantages of a 45° rim angle for parabolic solar dishes [27-33] which determined that it will lead to the highest concentration ratio and thermal performance [34].

2.6 Functional Parameters of Solar Parabolic Concentrators

The design of a parabolic dish concentrator is affected by many parameters which include the aperture diameter of the dish, the focal length of the parabolic concentrator, the aperture size of the receiver, the material of the reflector, the focal point diameter, the rim angle and the concentration ratio [35].

The sun an approximate blackbody with temperature of 5762K can emit a power density of 62.5 MW/m². The sun subtends an angle θ_S of approximately 0.53° and allows for a direct beam radiation of 800 to 100 W/m² at the surface of the earth [36].

The flux concentration C thermodynamic limit for a parabolic dish can be calculated using the following equation [37, 38].

$$C_{max} = \frac{1}{\sin^2\left(\frac{\theta_s}{2}\right)} \approx 45{,}000 \quad [1]$$

This equation is applicable only for air filled concentrators (no vacuum). The highest flux concentration that can be obtained by a dish is $C_{con,max}$ [39].

$$C_{con,max} = \frac{\sin^2(\frac{\theta_{rim}}{2})}{\sin^2(\frac{\theta_s}{2})} \quad [2]$$

The area concentration ratio can be calculated by dividing the area of the concentrator aperture over the area of the focal region, which is expressed by [34].

$$C = \frac{A_{con}}{A_{rec}} \quad [3]$$

Selection of the reflective material is an important parameter within the design considerations since it significantly affects the concentration of solar radiation onto the receiver. To calculate the energy input for a solar receiver the following equation can be used [35].

$$Q_{in} = CI\rho K \quad [4]$$

A solar parabolic dish has a unique geometry that enables it to concentrate solar radiation onto a small area, which increases its density and allows for high temperature accumulation. Parabolic dishes can be constructed based on the basic equation of a parabola that is [24],

$$y^2 = 4fx \quad [5]$$

The focal point of the parabolic concentrator is related to the rim angle and the diameter of the concentrator aperture. The rim angle can be defined as the angle measured at the focal point to the vertical axis connecting with the rim of the parabola [29]. The focal length of the parabola that leads to the focal point can be calculated using the following equations [35].

$$\frac{f}{D_{con}} = \frac{1}{4\tan\left(\frac{\theta_{rim}}{2}\right)} \quad [6]$$

$$h = \frac{D_{con}^2}{16f} \quad [7]$$

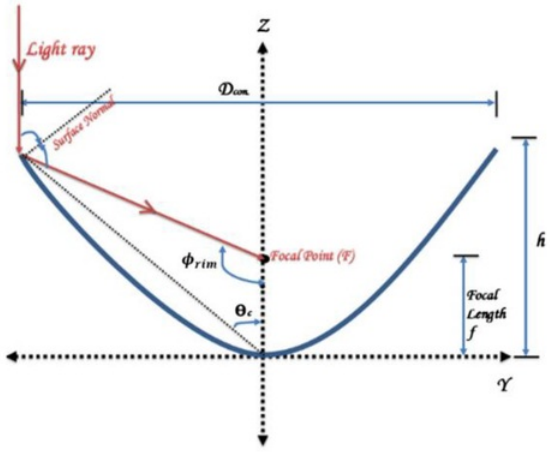

Figure 2.11 Parameters of parabolic dish [35].

The aperture area of the concentrator is defined as the surface area of which solar radiation is incident [40]. The size of this parameter will influence the amount of solar energy reflected towards the receiver. To determine the area of the aperture the following equation can be used [35].

$$A_{con} = \left(\frac{\pi}{4}\right) D_{con}^2 \quad [8]$$

The receiver size is highly influenced by the diameter of the focal point for the concentrated rays. The focal point diameter is related to the acceptance angle θ, the focal length f and the rim angle θ_{rim}. The acceptance angle is defined as the angle where maximum radiation is accepted without moving any part of the system. For higher concentration to be achieved a smaller angle is desired [38]. The focal point diameter can be calculated using the following equation [40].

$$D_{rec} = \frac{f\theta_{acc}}{cos\theta_{rim}(1 + cos\theta_{rim})} \quad [9]$$

Another formula which can determine the diameter for maximum concentration of receiver aperture [36].

$$D_{rec,max} = \frac{D_{con}(\frac{\theta_s}{2})}{2\tan(\frac{\theta_{rim}}{4})} \quad [10]$$

2.7 Review Conclusion

Parabolic dish systems have several advantages such as high-power density, durability for moisture, high efficiency and long lifetime. These systems are gaining attraction due to their easy design compared to other CSP technologies and many parts can be designed and manufactured by local manufacturers. In addition, their high concentration ratio can lead to high temperature concentration at lower cost compared to other CSP technologies [34]. Another main advantage for parabolic sysetms is that they have the least land requirement [13]. Wang and Siddiqui (2010), have also mentioned that parabolic dish systems are the most efficient concentrated solar power technologies which can achieve a concentration ratio of 10,000 suns. The high concentration will enable high efficiencies and thus higher temperatures than other CSP technologies. This advantage will allow these systems to be used for multiple applications such as thermochemical storage systems and the production of solar fuels [23]. Sup et al. (2015), have mentioned that parabolic systems have the ability to concentrated solar radiation to a temperature of 1500 C [24]. According Mancini et al. (2003), parabolic systems have proven to have the highest efficiency than other CSP technology by an approximate conversion rate of 30% of DNI solar radiation into electricity while considering parasitic power losses [15]. Finally Steinfeld and Romero (2012), have also mentioned that parabolic concentrators have a great advantage when integrated in large scale CSP plants since they exhibit high potential for scaling up in a cost-effective manner. They have also mentioned that a perfect parabolic concentrating can reach a maximum concentration ratio of 45,000 [12].

In the previous sections the key principles for thermochemical storage have been mentioned which include volumetric receivers and thermochemical processes. This research may be the a step for the development of a solar parabolic concentrator with thermochemical storage systems. As mentioned previous thermochemical processes require elevated temperatures, that can be achieved by parabolic dishes dues their high concentration characteristic. The purpose of this research is to study the effect of rim angles on parabolic systems and to determine methods for achieving the highest concentration.

CHAPTER 3

3 Experimental Setup and Procedure

3.1 Parabolic Dishes Model Development

In this experiment three parabolic dishes with a diameter of 300 mm but different rim angles (30°, 45° and 60°) were tested. Computer aided design on CREO Parametric was used to design the parabolic dishes. For the software to draw the correct parabolic shape, an equation had to be defined and inserted for each dish.

The diameter and rim angle for each dish has been decided therefore by using equation [6], the focal length can be calculated. The height of the parabola can be calculated using equation [7]. Equation [5] will define the shape of each parabolic shape on CREO Parametric. The dimensional values calculated for each dish are in *Table 3.1* below.

Table 3.1 Dimensions of parabolic dishes.

Dish Angle	Height (m)	Focal Length (m)	Equations
30°	0.02	0.28	$y = 0.000893x^2$
45°	0.031	0.181	$y = 0.001380x^2$
60°	0.043	0.13	$y = 0.001924x^2$

After the defining the equations, the dishes were designed as a solid part as seen in *Figure 3.1*. Two dimensional manufacturing drawings are given in Appendix A and can confirm the values for each calculation.

Figure 3.1 Parabolic dish design model.

When the three dimenionsal dish models were completed, they were exported as STL files for 3D printing as shown in *Figure 3.2*. Each dish will be 3-D printed on Omni3D using acrylonitrile butadiene styrene (ABS) as a base material. Omni3D has a print precision of 40 to 300 micrometres and is capable of printing parts up to 500 x 500 x 500 mm dimensions. The products were 3D printed models of parabolic dishes as shown in Figure 3.3.

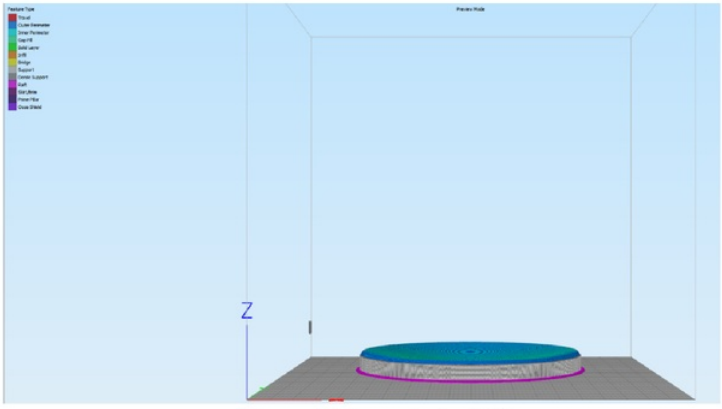

Figure 3.2 Imported stl file.

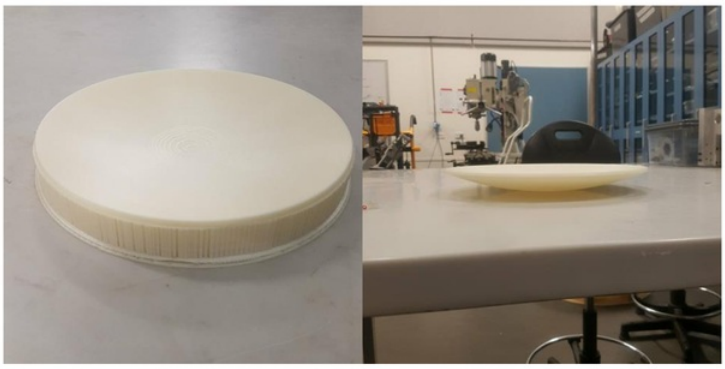

Figure 3.3 3-D printed dish.

After 3D printing the models, all the support material were taken off and the dishes were chrome plated to give a mirror surface finish. The results for this process can be seen in *Figure 3.4*, and
Figure 3.5 is a presentation of the 3 solar parabolic dish models to be tested.

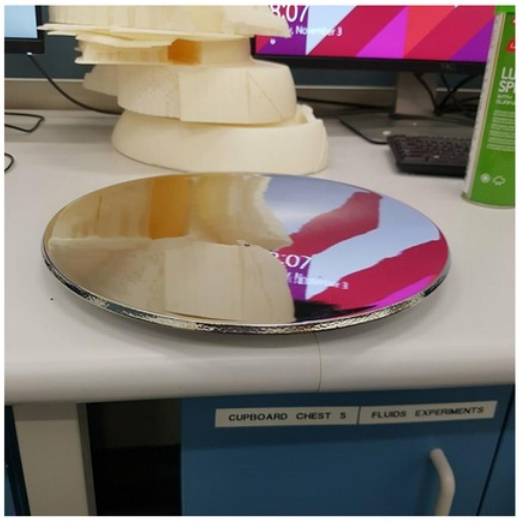

Figure 3.4 chrome plated parabolic dish.

Figure 3.5 All parabolic dishes to be tested.

3.2 Solar Simulator

The dishes were tested with a 300 W Xenon arc lamp (Y1089, Hidesada Toriyama Inc.) serving a solar simulator. The simulator is composed of two units as presented in *Figure 3.6*. The first unit (unit A) is the Xenon lamp which outputs a 5 cm of collimated light with solar characteristics. The second unit (unit B) is the current adjuster, which determines the power output of the lamp depending on the current.

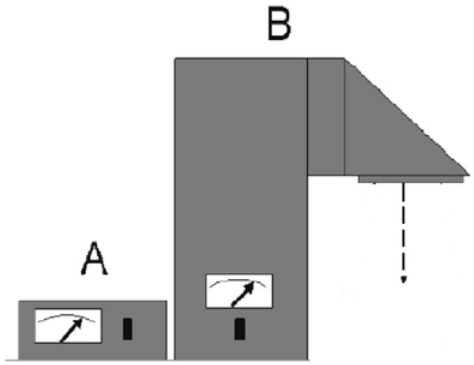

Figure 3.6 Solar simulator illustration.

Previous testing has showed the relation of current adjustment to the power output of the simulator. The results are shown in *Table 3.2* below.

Table 3.2 Current to power density adjustment.

Electric Current (A)	Power Density (mW/cm²)
10	8.14
15	351.76
20	671.14

It was decided to test the dishes at the previous mentioned currents and thus at their specific power output density.

The diameter of the light emitted by the lamp is 5 cm only and therefore it had to be expanded to reach the diameter of the dishes (30 cm). A Kaplerian beam expander was built as shown in *Figure 3.7* and hense expanding the beam to 300 mm.

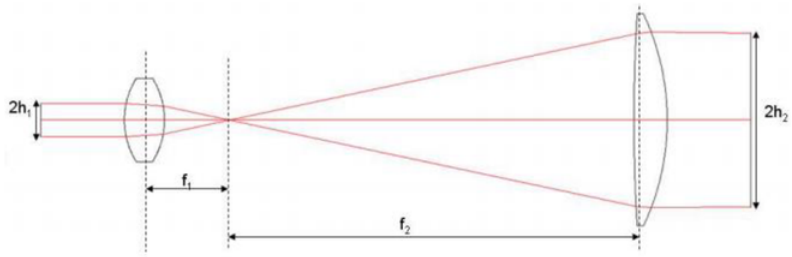

Figure 3.7 Kaplerian beam expander [41].

The beam expander is composed of two lenses, a converging lens and a Fresnel lens. A Fresnel lens is an optical device that can gather parallel rays onto a single focal point and conversely if light hits the lens while the source is located on its focal point, the output will be a collimated beam. A 317.5 mm diameter Fresnel lens can collimate light up to 300 mm which is suitable for this application. The other converging lens was selected based on the needed magnification of the solar simulator collimated beam. Equation [11] below will give a better understanding how magnification will affect the focal lengths for each lens.

$$M = \frac{F_2}{F_1} = \frac{h_2}{h_1} \qquad [11]$$

Where M is the magnification, F_2 and F_1 are the focal lengths for the Fresnel (large) lens and bi-convex (small) lens respectively. h_2 and h_1 represent half of the height for the beam exiting the Fresnel lens and entering the bi-convex lens respectively. These parameters can be observed in *Figure 3.7*. The beam has to be expanded from 50 mm to 300 mm, then a magnification with a value of 6 is required. The effective focal length of the chosen Fresnel lens is 584.2 mm. Therefore, by using the magnification value and effective focal length value of the Fresnel lens, then by using equation [11] the effective focal length value can be calculated for the converging lens. Calculation gives a value of 97 mm focal length, which was the basis for acquiring the converging lens. Spacing between the two lenses should be the sum of the two focal lengths, which is 681.5 mm. Combining everything together as shown in *Figure 3.8*, the solar simulator will output a 50 mm diameter beam that will enter the converging lens, then light will expand to 300

mm when it reaches the Fresnel lens and finally collimated rays will exit the Fresnel lens to hit the parabolic dish. The dish will focus the incident rays at a focal point.

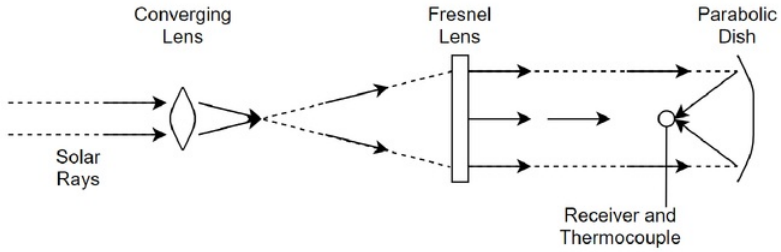

Figure 3.8 Sketch of testing procedure 1.

3.3 Testing Rig Development

An experimental setup has been designed and assembled for testing the parabolic dish models. The experimental setup is made up from several parts and the function of each part will be illustrated in this section. A 3D representation of the experimental setup is shown in *Figure 3.9*.

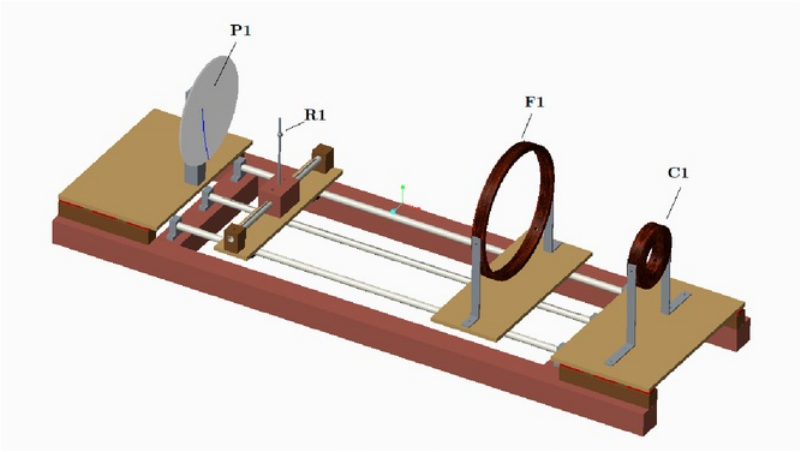

Figure 3.9 Testing rig model.

C1 and F1 are the concave and Fresnel lens holders respectively. The concave lens holder sits on a fixed platform while the other lens is mounted on a moving platform via linear bearings. C1 and F1 should be 681.5 mm apart to achieve a beam magnification to the value of 6. The lens holders are milled from a circular wooden board as shown in *Figure 3.10*. The holes in the holders are threaded, this will enable to fix the lenses by using bolts.

Figure 3.10 Lens holders model.

P1 is the parabolic dish and should be perfectly aligned to the two lenses as shown *Figure 3.11*. The center of the dish, concave lens, Fresnel lens and receive was designed to 230 mm above the platform. R1 is the receiver model of the system and it can slide on linear bearings similarly to F1. R1 will act as the receiver of the parabolic dish and it is a 15 mm sphere made from lead. Each dish has a different focal length at which incident rays is focused, therefore R1 can slide and overlap the focal point of each dish.

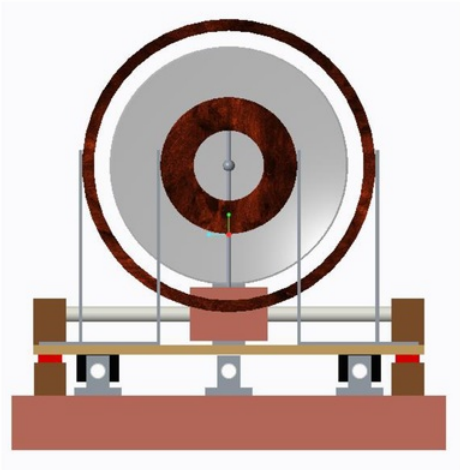

Figure 3.11 Testing rig front view.

This testing rig was designed to test parabolic dish models up to 400 mm in diameter. A side and top view for the testing rig is shown in *Figure 3.12* and *Figure 3.13*. This testing rig can study the relation between the rim angles and diameter of the dish. In addition it will be able to study the effect of receivers with different geometries on the concentration ratio of the system. In this experiment only the effects of the rim angle will be tested while the receiver R1 will only act as a temperature measuring tool.

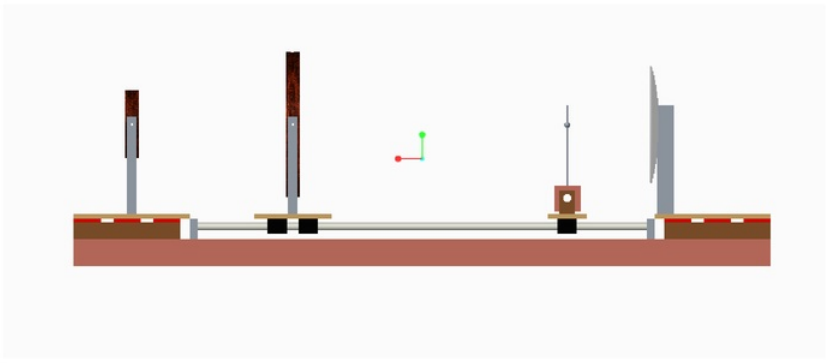

Figure 3.12 Testing rig side view.

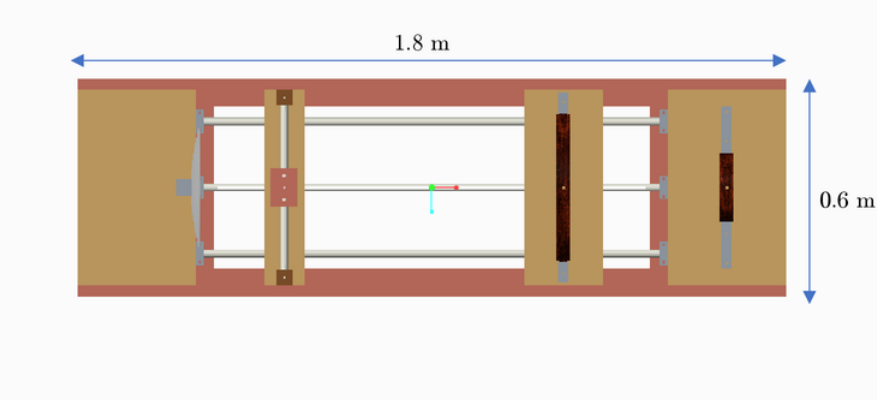

Figure 3.13 Testing rig top view.

3.4 Testing Procedure

Before testing started the experiment had to be setup as shown in *Figure 3.14*. Below is a list of steps done during the experimental setup and experimental procedure.

- The 317.5 mm and 79.4 mm diameters Fresnel and converging lens were mounted in their holders respectively.
- The Fresnel lens was fixed 681.5 mm away from the converging lens.
- The centre of the simulator lens was aligned to the center of the converging lens as shown in *Figure 3.15*.
- The solar simulator was turned on for 15 min before testing without activating the lamp and the current was caliberated to 10 A.
- The first parabolic dish was mounted.
- The receiver was fixed at the focal point of the parabolic dish.
- A RS-1327K thermocouple was fixed at the receiver to measure the temperature.
- Room temperature was noted.
- Initial temperature of the receiver was noted.

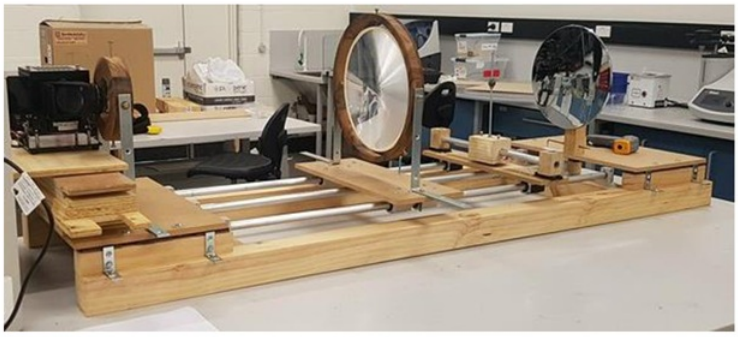

Figure 3.14 Assembled testing rig.

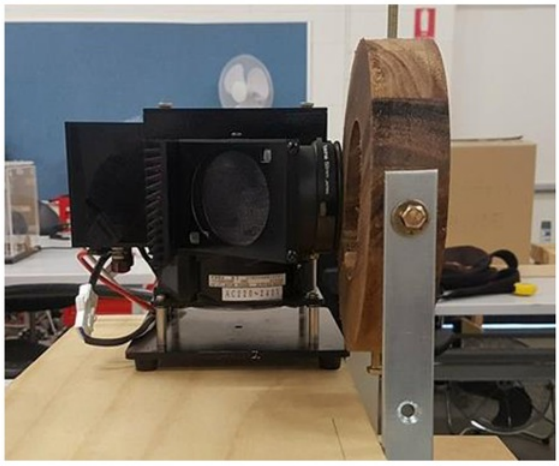

Figure 3.15 Solar simulator lamp aligned to concave lens.

The 30° rim angle dish was first tested at 10 A current. After the initial temperature of the lead receiver was noted, the lamp was switched on as seen in *Figure 3.16*. During the first minute, temperature was recorded every 10 seconds. After the first minute and until 8 minutes, temperature was recorded every 15 seconds. From minute 8 to minute 20, temperature was recorded in 30 second increments. The last 15 minutes were recorded in 1 min increments. The experiment was stopped at 35 minutes when the final temperature has stabilized.

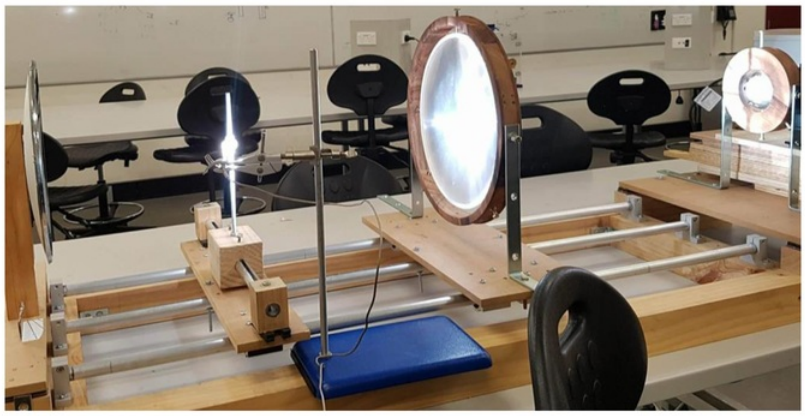

Figure 3.16 Functioning testing rig

The same procedure was done for the 15 A and 20 A adjustment. The procedure was also redone for the 45° and 60° rim angle dishes at three current adjustments, 10, 15 and 20 A. In all of the experiments temperature was recorded in the exact same manner as done for the 30° rim angle at 10 A current adjustment.

Another test was done without using any dish and that is for measuring the temperature of the incident solar rays at the three different current adjustments. The same procedure was applied for this test but the only difference is that the thermocouple is not measuring the concentrated rays, but the temperature of the incident rays. This can be done by placing the thermocouple right after the Fresnel lens. This test is represented in *Figure 3.17*.

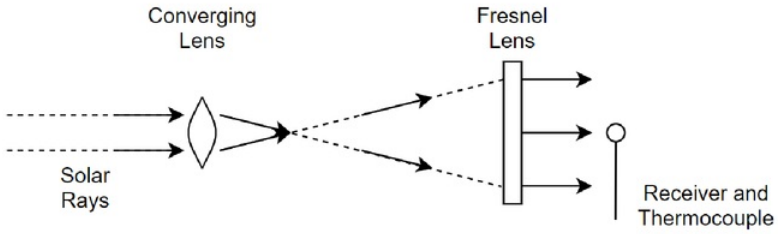

Figure 3.17 Sketch of testing procedure 2.

A final test was done to measure the maximum temperature of the solar simulator output at each current adjustment. This was done by concentrating the beam from the simulator with the converging lens on a thermocouple as seen in *Figure 3.18*.

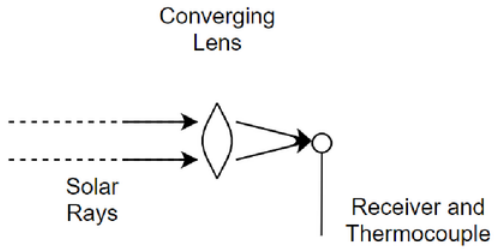

Figure 3.18 Sktech of testing procedure 3.

CHAPTER 4

4 Results and Discussion

As mentioned previously each current adjustment in the solar simulator will give a specific power density and this can be referred to *Table 3.2*. The solar simulator will output a beam with 5 cm diameter. Therefore, by updating *Table 3.2* the power output for each current adjustment can be determined as seen in *Table 4.1*. For simplicity

purposes, the power density and power outputs of the solar simulator may be mentioned by their current adjustment.

Table 4.1 Power output specific for each power density.

Electric Current (A)	Power Density (mW/cm²)	Power Output (W)
10	8.14	0.15983
15	351.76	6.90679
25	671.14	13.1778

All the results show an exponential increase before reaching a stabilized temperature. The concentrated solar power output of the simulator at three different power densities is given in *Figure 4.1*. It is evident in the figure of a rapid increase in temperature before stabilizing. The final temperature can be assumed by taking the average of the last 10 values from the graph. Therefore, the temperature values at each power density is given in *Table 4.2*.

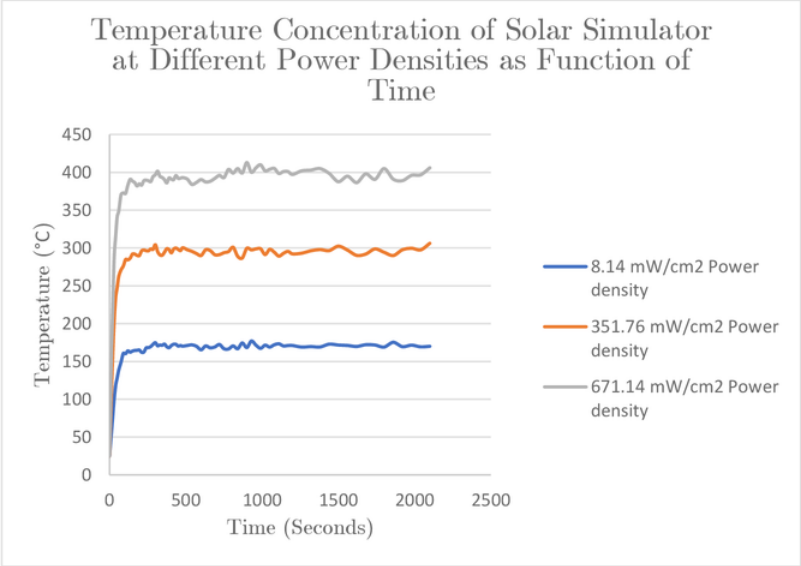

Figure 4.1 Temperature concentration of solar simulator at different power densities.

Table 4.2 maximum achieved temperature for concentrated solar simulator power at different power densities.

Power Density (mW/cm²)	Temperature Concentration (°C)
8.14	170.93
351.76	296.33
651.14	395.37

The temperature of the incident rays was measured at different power density outputs. The results are shown in *Figure 4.2*. The final temperature can be assumed by taking the average of the last 10 values from the graph. Therefore, the temperature values at each current adjustment is given in *Table 4.3*.

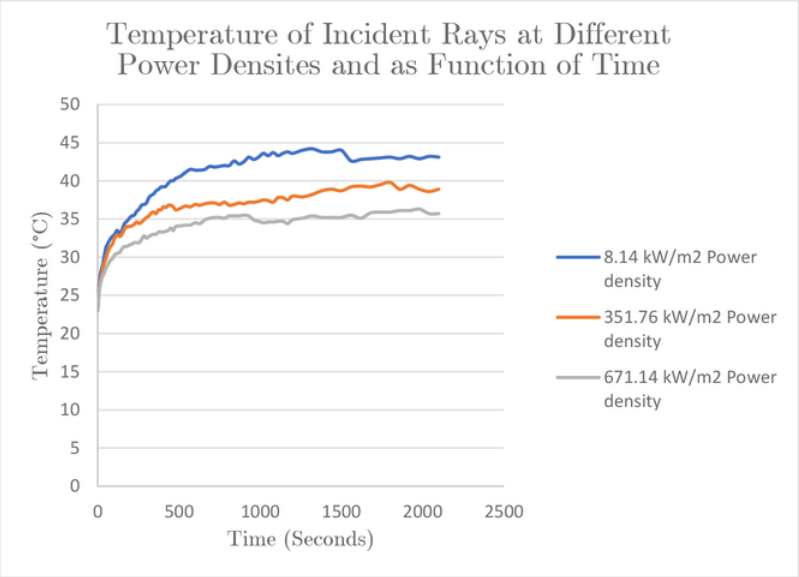

Figure 4.2 Temperature of incident field

Table 4.3 Temperature of incident field

Power Density (mW/cm²)	Temperature Concentration (°C)
8.14	35.81
351.76	39.17
671.14	42.97

The concentrated rays from the parabolic dishes also cause an exponential increase in temperature as shown in *Figure 4.3* to *Figure 4.5*. The final temperatures can be assumed by taking the average of the last 10 values from the graphs. Therefore, the temperature values at each current adjustment is given in *Table 4.4* for all parabolic dishes.

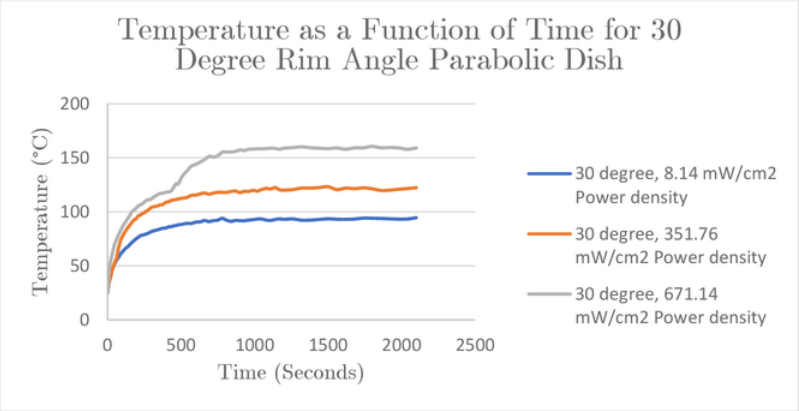

Figure 4.3 Temperature as a function of time for 30 degree rim angle parabolic dish

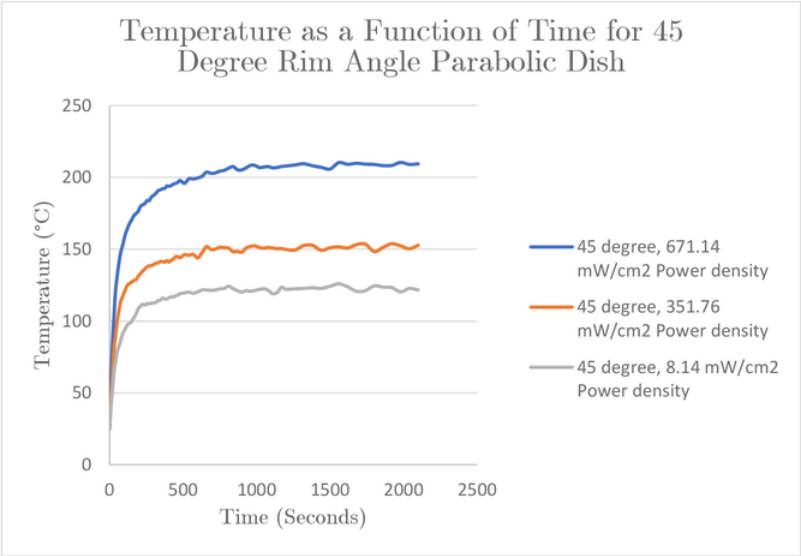

Figure 4.4 Temperature as a function of time for 45 degree rim angle parabolic dish

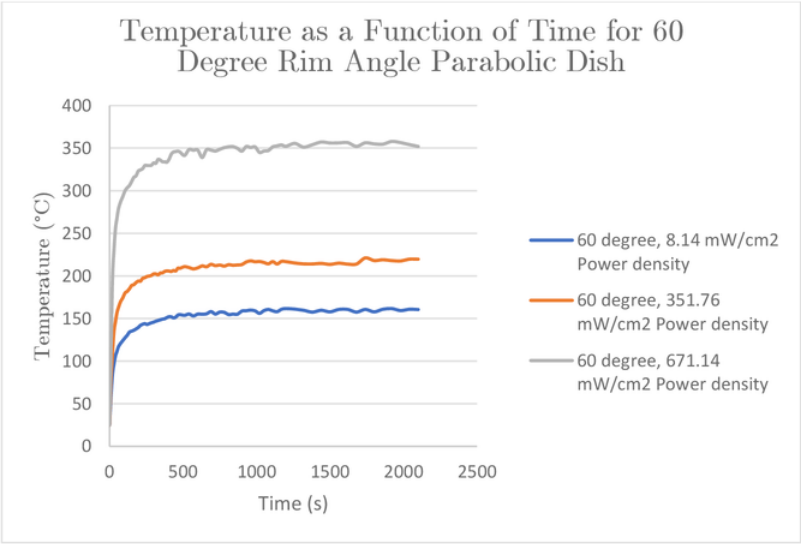

Figure 4.5 Temperature as a function of time for 60 degree rim angle parabolic dish

Table 4.4 Concentrated temperature for each dish at a specific power density

Parabolic Dish Rim Angle	Power density (mW/cm²)	Concentrated Temperature (°C)
30°	8.14	93.68
	351.76	121.25
	671.14	159.13
45°	8.14	122.74
	351.76	151.77
	671.14	209.27
60°	8.14	160.11
	351.76	217.62
	671.14	355.14

The resultant temperature of each test are shown in *Table 4.5*. The temperatures for each testing condition were plotted against the power density output of the solar simulator in *Figure 4.6*. The graph shows a linear relationship between incident temperature and power output of the solar simulator, which can be given by the equation.

$$y = 0.0108x + 35.61$$

The graph also shows a linear relationship after the rays were concentrated using a converging lens, which is given by.

$$y = 0.3389x + 171.09$$

This linearity is not seen when the solar rays were concentrated using the parabolic dishes. In fact linearity decreases when the rim angle of the parabolic dishes increases this is evident in *Figure 4.6*.

Table 4.5 Final temperature for each test.

Power Output of Solar Simulator (mW/cm²)	30° Dish (°C)	45° Dish (°C)	60° Dish (°C)	Incident Rays (°C)	Concentrated Temperature of Solar Simulator (°C)
8.14	93.68	122.74	160.11	35.81	170.93
351.76	121.25	151.77	217.62	39.17	296.33
671.14	159.13	209.27	355.14	42.97	395.37

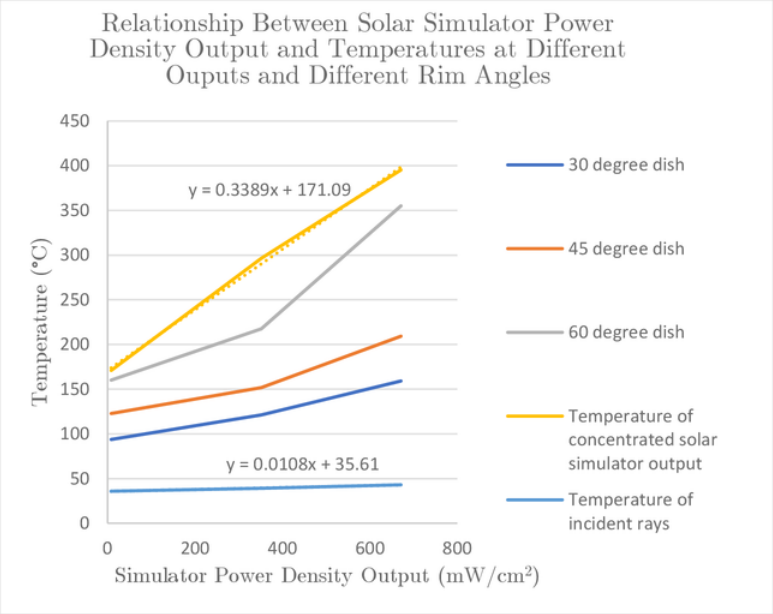

Figure 4.6 Relationship between solar simulator power density output and temperatures at different ouputs and different rim angles

Looking at *Figure 4.3* to *Figure 4.5*, it is realized that the temperature gap between the power density outputs of 351.76 kW/m² and 671.14 kW/m² is larger than when the power density output was between 8.14 kW/m² and 351.76 kW/m².

It is assumed that the radiated area of the lead (Pb) receiver is the same for all cases. This will enable to analyse the results based on the radiative heat transfer. The Pb receiver is assumed to be a grey body (non black body), which has characteristics of absorption, transmittance and reflection. This will allow the use of Stefan-Boltzmann Law which is given by.

$$Q_{rad} = \varepsilon\sigma T^4 A \qquad [12]$$

Since the power flux density will be used for the analysis, this equation will become.

$$Q_{rad}/A = \varepsilon\sigma T^4 \quad [13]$$

The emissivity of oxidized Pb is 0.63 [42]. The temperature on the Pb surface is given for each testing condition, therefore by using equation 13, the results in *Table 4.6* were achieved.

Table 4.6 Radiative heat transfer for each test.

Testing Conditions	Power Density (mW/cm^2)	Temperature (°C)	Radiative Heat Transfer (W/m^2)
Concentrated Rays from Solar Simulator	8.14	170.93	30.49438
	351.76	296.33	275.454
	671.14	395.37	872.8939
Incident Rays	8.14	35.81	0.058744
	351.76	39.17	0.084093
	671.14	42.97	0.121789
Concentrated Rays from 30° Parabolic Dish	8.14	93.68	2.751276
	351.76	121.25	7.721
	671.14	159.13	22.90629
Concentrated Rays from 45° Parabolic Dish	8.14	122.74	8.107577
	351.76	151.77	18.95354
	671.14	209.27	68.51324
Concentrated Rays from 60° Parabolic Dish	8.14	160.11	23.4758
	351.76	217.62	80.12016
	671.14	355.14	568.2572

Radiative heat transfer efficiency was determined by finding the maximum radiative heat transfer by the system. This is determined by the temperature of the concentrated rays from the solar simulator, divided by the radiave heat transfer at the receiver for the parabolic dishes. The radiative transfer efficiency is given by.

$$\alpha_{Qrad,eff} = \frac{Q_{rad,rec}}{Q_{rad,solar\ simulator}} \times 100 \quad [14]$$

The radiative transfer ratio for was determined by finding the radiative heat transfer of the incident rays which was calculated using the temperature of the thermocouple at that point. Then by dividing the radiative heat transfer of the receiver over the value related to the incident rays. The radiative transfer ratio can be determined by.

$$R_{rad} = \frac{Q_{rad,rec}}{Q_{rad,incident}} \quad [15]$$

The results for the radiative transfer efficiency are in *Table 4.7*. Plotting these results in *Figure 4.7* shows that the dish having 60° rim angle has a significantly higher efficiency than both the 30° and 45° rim angles. But depending on the power output from the solar simulator received by the dish, this efficiency changes. The efficiency is maximum at minimum power density output from the solar simulator (8.14 mW/cm^2) for the parabolic dishes. The efficiency drops to minimum when the power output by the simulator is 351.76 mW/cm^2 then rises when the solar simulator is adjusted to maximum power density (671.14 mW/cm^2). The radiation transefer ratio is maximum at maximum power output of the simulator for all parabolic dishes, but the most significant increase was noticed for the 60° rim angle parabolic dish which increases to reach maximum radiation concentration of approximately 4666. The results for the radiation transfer ratio are plotted in *Figure 4.8*.

Table 4.7 Radiative transfer efficiency and ratio

Testing Conditions	Power Density (mW/cm^2)	Radiative Transfer Efficiency (%)	Radiative Transfer Ratio
Concentrated Rays from 30° Parabolic Dish	8.14	9.0222	46.8350
	351.76	2.8030	91.8148
	671.14	2.6242	188.0818
Concentrated Rays from 45° Parabolic Dish	8.14	26.587	138.0153
	351.76	6.8808	225.3873
	671.14	7.8490	562.5570
Concentrated Rays from 60° Parabolic Dish	8.14	76.9840	399.6286
	351.76	29.0866	952.7543
	671.14	65.1004	4665.9163

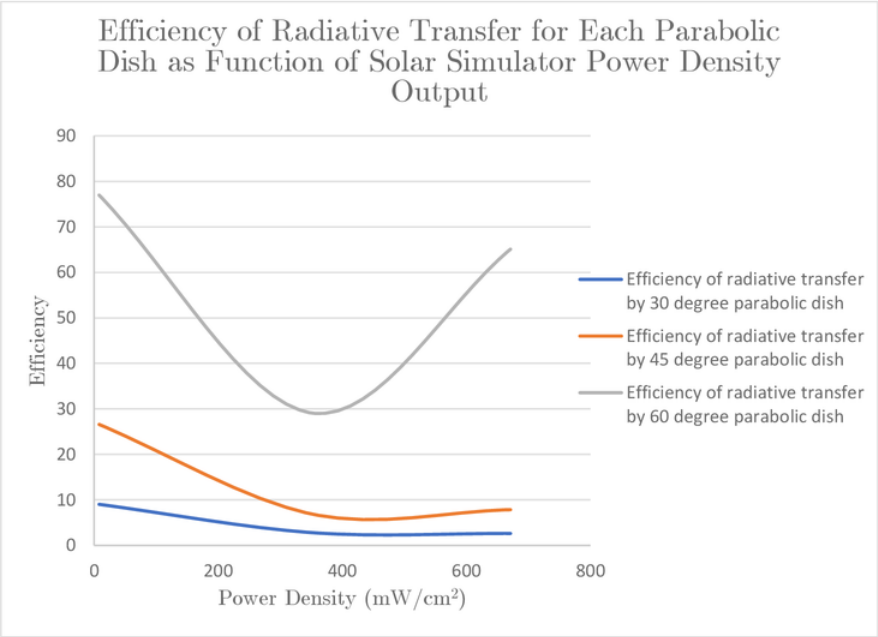

Figure 4.7 Efficiency of radiative transfer for each parabolic dish as function of solar simulator power density output

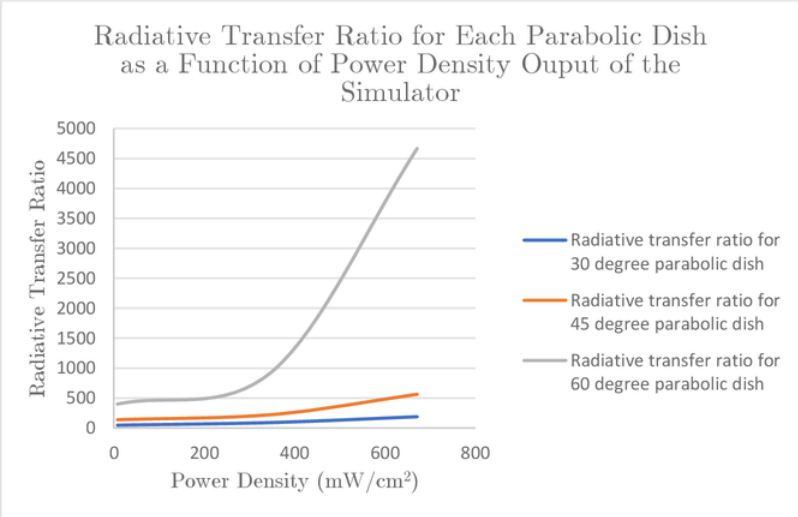

Figure 4.8 Radiative transfer ratio for each parabolic dish as a function of power density ouput of the simulator

Another analysis has been made to observe the relation between the rim angle and radiation transfer ratio and between that rim angle and the efficiency of the system. This analysis can be observed graphically in *Figure 4.9* and *Figure 4.10*. At lower power outputs of the simulator it can be seen that there is a relationship almost approaching linearity, specifically at 8.14 mW/cm². This relationship dissipates for other simulator power density outputs.

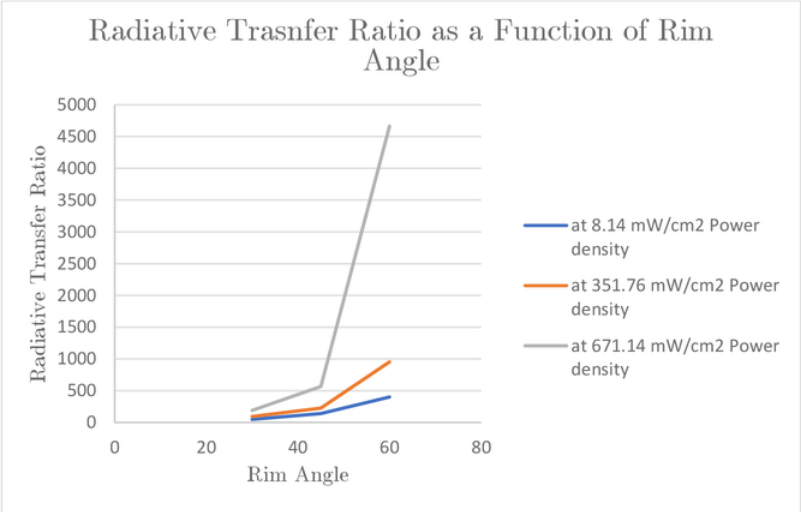

Figure 4.9 Radiative trasnfer ratio as a function of rim angle

Figure 4.10 Efficiency as a function of rim angle

Analysing the system based on convection will enable to determine the concentration ratio of the parabolic dish. The equation that will define the convective heat transfer in the system is given by,

$$Q_p A_{dish} \rho \delta = h A_{rec} (T_{max} - T_{min}) \quad [16]$$

Where Q_p is density power output of the simulator. The power density entering the parabolic dish is assumed to be equal to be power density output of the solar simulator. For calculation purposes the density is expressed in W/m^2 in this analysis.The surface area of the dish A_{dish} can be calculated using equations for surface area of a parabolic shape. The equation is given by.

$$A_{dish} = \frac{\pi r}{6h^2}(r^2 + 4h^2)^{\frac{3}{2}} - r^3 \quad [17]$$

The surface area for each dish is given in *Table 4.8*. ρ and δ are the reflectivity and absorptivity of the material, respectively, which are determined to be 0.7 and 0.2 for a chrome plated surfaces [43, 44]. The heat transfer coefficient of air is assumed to 100 W/m^2K. T_{max} is the maximum achieved temperature by each dish at a specific density power output of the simulator. T_{min} is the ambient temperature of the

receiver. By rearranging equation 17 and substituting all known values, the surface area of concentration can be determined.

Table 4.8 Surface area for each dish

Parabolic dish	Power Density (W/m^2)	Height (m)	Radius (m)	Surface Area of Dish (m^2)
30°	81.4	0.02	0.15	0.071927962
	3517.6	0.02	0.15	0.071927962
	6711.4	0.02	0.15	0.071927962
45°	81.4	0.031	0.15	0.073624019
	3517.6	0.031	0.15	0.073624019
	6711.4	0.031	0.15	0.073624019
60°	81.4	0.043	0.15	0.076210206
	3517.6	0.043	0.15	0.076210206
	6711.4	0.043	0.15	0.076210206

The surface area of concentration was determined in *Table 4.8*. To find the concentration ratio relative to each rim angle, equation [3] can be used. The surface area of the parabolic dish aperture (A_{con}) is equal to $\pi(0.15)^2$. The concentration ratio is given in *Table 4.9* after dividing aperture surface area of each dish by the surface area of concentration.

Table 4.9 Concentration ratio for each dish

Angle	Temperature (°C)	Area of concentration (m^2)	Concentration Ratio
30°	93.68	0.000119349	592.2601089
	121.25	0.003680201	19.20705969
	159.13	0.005038636	14.02876375
45°	122.74	8.5842E-05	823.4415209
	151.77	0.002860076	24.71467307
	209.27	0.003754102	18.8289605
60°	160.11	6.42803E-05	1099.649563
	217.62	0.001948436	36.27823441
	355.14	0.002168983	32.58939065

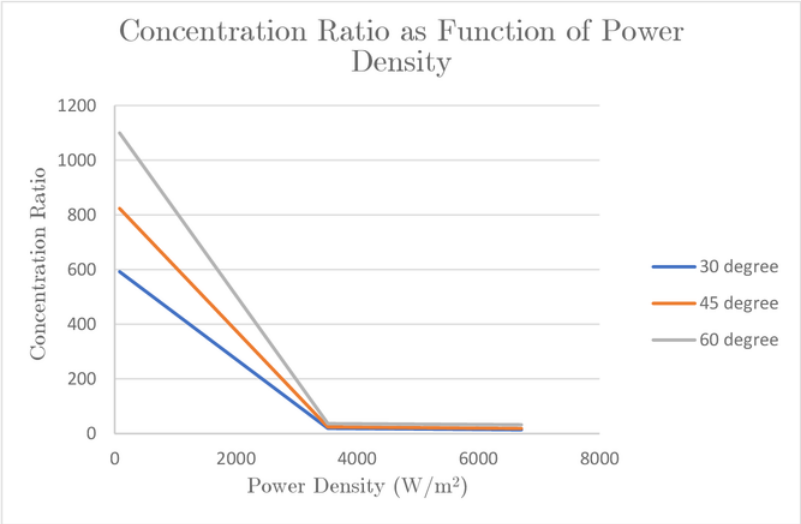

Figure 4.11 Concentration ratio as function of power density

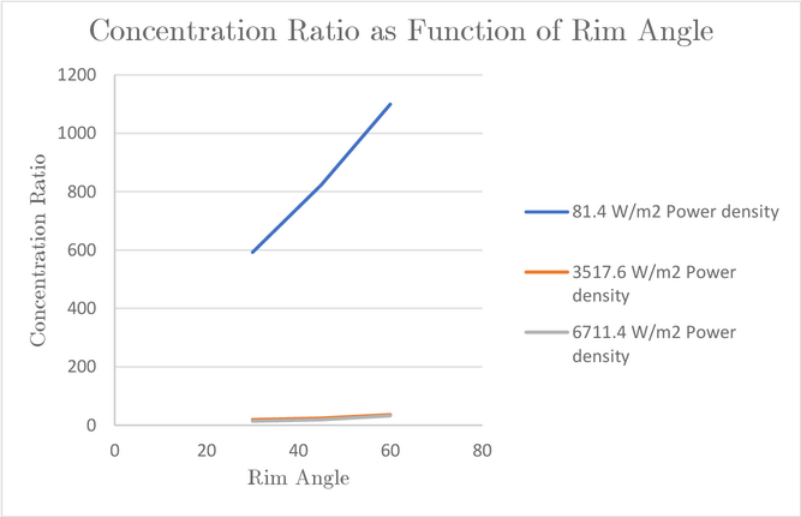

Figure 4.12 Concentration ratio as function of rim angle

According to the results obtained in this experiment it can be concluded that the efficiency and radiation concentration increases when the rim angle of the parabolic dish is higher. This is evident from the discussed results, since the 60° rim angle parabolic dish has the

highest efficiency and thermal radiation performance. But the highest efficiency drop was evident in the 60° rim angle, as can be seen in *Figure 4.7*. A relationship can be determined between the radiation received and the efficiency drop for different rim angles. As the rim angle of the parabolic dish decreases its efficiency increases, since the 30° rim angle dish has the lowest efficiency drop. Efficiency drop can be explained as the performance of the system during various DNI received by the dish, since DNI depends on many factors such as weather, season and landscape elevation. Plotting the results in *Figure 4.11* shows the relationship between the concentration ratio and density power output of the simulator. As the power density output of the simulator increases the concentration ratio decreases. *Figure 4.12* is a representation of the relationship between the concentration ratio and the rim angle of each. Even at various power outputs of the simulator, the concentration ratio increases with increasing angle. The results have shown that as the angle increases, the concentration ratio and thermal performance of the system also increases. The literatures discussed previously in the background favoured the use of a 45° rim angle since it provides the best compensation between efficiency and thermcal performance. According to those literatures, the simulations was done based on integrating Stirling or Brayton engines. The purpose of this research was to achieve the highest concentration possible, that will enable incorporating thermochemical storage systems to small scale size parabolic dishes. The results of this experiment proved that the 60° rim angle may achieve the highest thermal radiation compared to other tested angles. The thermal radiation analysis confirms the results obtained by the concentration ratio analysis, since the highest radiative heat transfer occurred at 60°.

CHAPTER 5

5 Conclusion

In this research the effect of the rim angle on the parabolic dish was investigated based on other studies. A testing rig was developed to test three parabolic dishes with different rim angles (30°, 45° & 60°), but with the same diameter. It can be concluded that a 60° rim angle can achieve the highest concentration ratio and thermal performance, and thus it is more suitable for concentrated solar power applications that require high temperatures. The literatures mentioned that a 45 rim can angle provide the best compensation between concentration and efficiency. This was seen in this experiment, since the drop in efficiency as lower than that of a 60° angle. Although this efficiency will affect the performance of the system, but it will still remain higher than angles with a lower value. In conclusion, the 60° angle may be the most appropriate angle for a small scale CSP plant.

CHAPTER 6

6 Impact and Future Work

This research has provided a deeper understanding on the effect of rim angles on concentration and efficiency of parabolic concentrators. As mentioned previously a large population of the world still live without the availability of electricity. This research may be a step in the development of a small scale portable parabolic concentrator that can provide electricity for small settlements or rural areas in Asia and Africa. A 60° rim angle parabolic dish has proven to have a high concentration characteristics, therefore future work can be done through simulations on larger scale dishes integrated with thermochemical receiver models.

7 Appendix A

Two-dimensional drawings of the parabolic dish models.

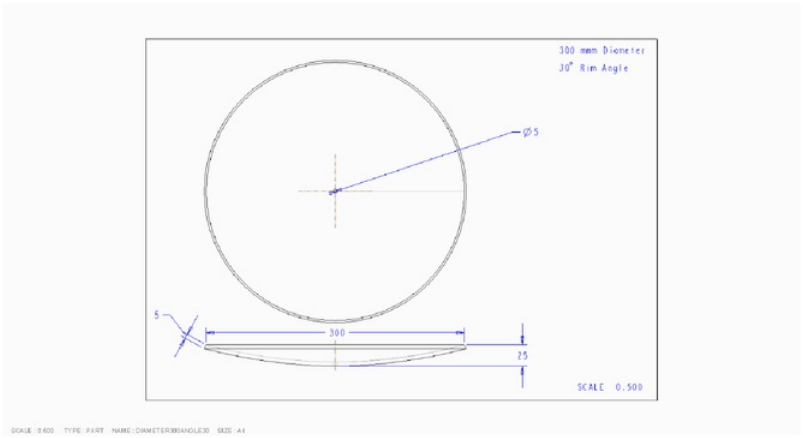

Figure 7.1 300 mm parabolic dish, 30 degree rim angle

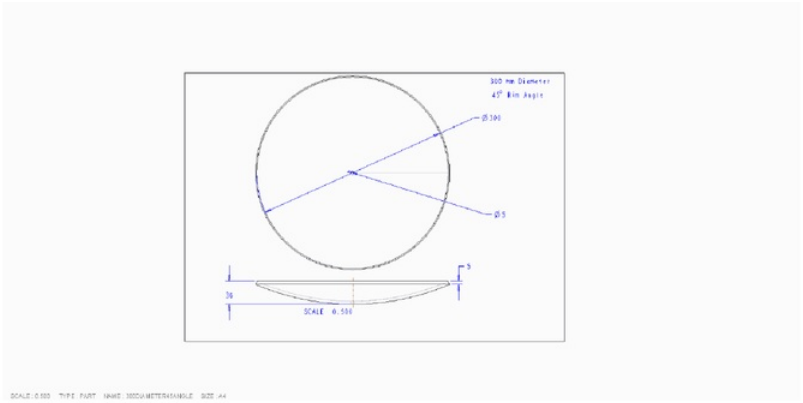

Figure 7.2 300 mm parabolic dish, 45 degree rim angle

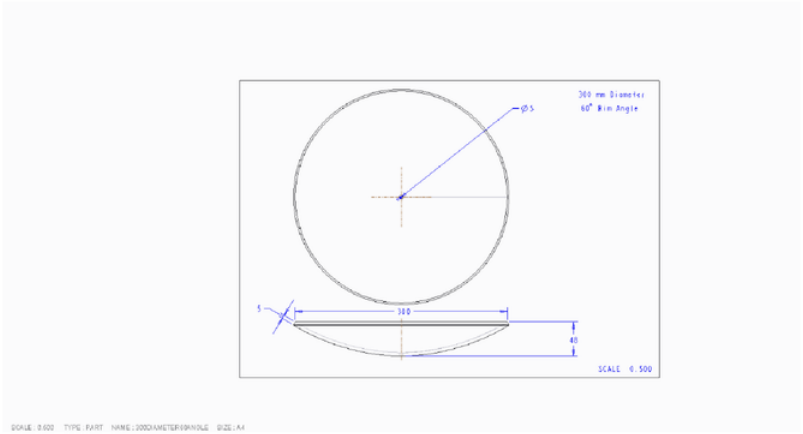

Figure 7.3 300 mm parabolic dish, 60 degree rim angle.

References

[1] I. E. Agency, *Technology Roadmap Solar Thermal Electricity*, International Energy Agency, 9 rue de la Federation 75739 Paris Cedex 15, France, 2014.

[2] I. E. Agency, *World Energy Outlook*, 9 rue de la Federation 75739 Paris Cedex 15, France: Organization for Economic Cooperation & Development London, 2015.

[3] IRENA, *Rethinking Energy 2017*, Abu Dhabi, 2017.

[4] IEA, and IRENA, *Prespective For The Energy Transition: Investment Needs for a Low-Carbon Energy-System*, 2017.

[5] M. R. Moore, G. M. Lewis, and D. J. Cepela, "Markets for renewable energy and pollution emissions: Environmental claims, emission-reduction accounting, and product decoupling," *Energy Policy,* vol. 38, no. 10, pp. 5956-5966, 2010.

[6] I. Purohit, and P. Purohit, "Techno-economic evaluation of concentrating solar power generation in India," *Energy Policy,* vol. 38, no. 6, pp. 3015-3029, 2010.

[7] Z.-Y. Zhao, Y.-L. Chen, and J. D. Thomson, "Levelized cost of energy modeling for concentrated solar power projects: A China study," *Energy,* vol. 120, pp. 117-127, 2017.

[8] S. Karekezi, and W. Kithyoma, "Renewable energy strategies for rural Africa: is a PV-led renewable energy strategy the right approach for providing modern energy to the rural poor of sub-Saharan Africa?," *Energy Policy,* vol. 30, no. 11-12, pp. 1071-1086, 2002.

[9] J. Clifton, and B. J. Boruff, "Assessing the potential for concentrated solar power development in rural Australia," *Energy Policy,* vol. 38, no. 9, pp. 5272-5280, 2010.

[10] R. Tamme, R. Buck, M. Epstein, U. Fisher, and C. Sugarmen, "Solar Upgrading of Fuels for Generation of Electricity," *Journal of Solar Energy Engineering,* vol. 123, no. 2, 2001.

[11] ATKearney, and ESTELA, *Solar Thermal Electricity 2025*, June 2010.

[12] M. Romero, and A. Steinfeld, "Concentrating solar thermal power and thermochemical fuels," *Energy & Environmental Science,* vol. 5, no. 11, 2012.

[13] H. L. Zhang, J. Baeyens, J. Degrève, and G. Cacères, "Concentrated solar power plants: Review and design methodology," *Renewable and Sustainable Energy Reviews,* vol. 22, pp. 466-481, 2013.

[14] CleanLeap. "Solar Thermal Technology," 4 October 2017; http://cleanleap.com/7-solar-technology-assessment-and-appropriate-technology-options/71-solar-thermal-technology.

[15] T. Mancini, P. Heller, B. Butler, B. Osborn, W. Schiel, V. Goldberg, R. Buck, R. Diver, C. Andraka, and J. Moreno, "Dish-Stirling Systems: An Overview of Development and Status," *Journal of Solar Energy Engineering,* vol. 125, no. 2, 2003.

[16] A. Steinfeld, and R. Palumbo, "Solar Thermochemical Process Technology," *Encyclopedia of Physical Science and Technology,* vol. 15, pp. pp. 237-256, 2001.

[17] D. Yadav, and R. Banerjee, "A review of solar thermochemical processes," *Renewable and Sustainable Energy Reviews,* vol. 54, pp. 497-532, 2016.

[18] A. Steinfeld, "Solar thermochemical production of hydrogen—a review," *Solar Energy,* vol. 78, no. 5, pp. 603-615, 2005.

[19] D. S. A. Simakov, M. M. Wright, S. Ahmed, E. M. A. Mokheimer, and Y. Román-Leshkov, "Solar thermal catalytic reforming of natural gas: a review on chemistry, catalysis and system design," *Catal. Sci. Technol.,* vol. 5, no. 4, pp. 1991-2016, 2015.

[20] P. Furler, J. R. Scheffe, and A. Steinfeld, "Syngas production by simultaneous splitting of H2O and CO2via ceria redox reactions in a high-

temperature solar reactor," *Energy Environ. Sci.,* vol. 5, no. 3, pp. 6098-6103, 2012.

[21] A. Steinfeld, M. Brack, A. Meier, A. Weidenkaff, and D. Wuillemin, "A solar chemical reactor for co-production of zinc and synthesis gas," *Energy,* vol. 23, no. 10, pp. 803-814, 1998.

[22] R. Buck, J. F. Muir, and R. E. Hogan, "Carbon dioxide reforming of methane in a solar volumetric receiver/reactor: the CAESAR project," *Solar Energy Materials,* vol. 24, no. 1-4, pp. 449-463, 1991.

[23] M. Wang, and K. Siddiqui, "The impact of geometrical parameters on the thermal performance of a solar receiver of dish-type concentrated solar energy system," *Renewable Energy,* vol. 35, no. 11, pp. 2501-2513, 2010.

[24] B. A. Sup, M. F. Zainudin, T. Z. S. Ali, R. A. Bakar, and G. L. Ming, "Effect of Rim Angle to the Flux Distribution Diameter in Solar Parabolic Dish Collector," *Energy Procedia,* vol. 68, pp. 45-52, 2015.

[25] R. Beltran, N. Velazquez, A. C. Espericueta, D. Sauceda, and G. Perez, "Mathematical model for the study and design of a solar dish collector with cavity receiver for its application in Stirling engines," *Journal of Mechanical Science and Technology,* vol. 26, no. 10, pp. 3311-3321, 2012.

[26] J. A. Harris, and T. G. Lenz, "Thermal performance of solar concentrator/cavity receiver systems," *Solar Energy,* vol. 34, no. 2, pp. 135-142, 1985.

[27] I. L. Mohammed, "Design and Development of a Parabolic Dish Solar Water Heater," *International Journal of Engineering Research and Applications,* vol. 2, no. 1, pp. 822-830, 2012.

[28] D. Howard, and R. G. Harley, "Modeling of dish-Stirling solar thermal power generation," 2010.

[29] W. B. Stine, and R. B. Diver, *A compendium of solar dish/Stirling technology*, Sandia National Laboratories, 1994.

[30] P. R. Fraser, "Stirling dish system performance prediction model," Mechanical Engineering Department, University of Wisconsin, 2008.

[31] W. Reinalter, S. Ulmer, P. Heller, T. Rauch, J. M. Gineste, A. Ferriere, and F. Nepveu, "Detailed Performance Analysis of a 10 kW Dish/Stirling System," *Journal of Solar Energy Engineering,* vol. 130, no. 1, 2008.

[32] M. Li, and J. Dong, "Modeling and Simulation of Solar Dish-Stirling Systems."

[33] W. Schiel, and T. Keck, "Parabolic dish concentrating solar power (CSP) systems," *Concentrating Solar Power Technology*, pp. 284-322, 2012.

[34] A. Z. Hafez, A. Soliman, K. A. El-Metwally, and I. M. Ismail, "Design analysis factors and specifications of solar dish technologies for different systems and applications," *Renewable and Sustainable Energy Reviews,* vol. 67, pp. 1019-1036, 2017.

[35] A. Z. Hafez, A. Soliman, K. A. El-Metwally, and I. M. Ismail, "Solar parabolic dish Stirling engine system design, simulation, and thermal analysis," *Energy Conversion and Management,* vol. 126, pp. 60-75, 2016.

[36] D. Feuemann, and J. M. Gordon, "High-concentration collection and remote delivery of sunlight with fiber optic minidishes."

[37] W. T. Welford, and R. Winston, *High Collection Nonimaging Optics*, San Diego: Academic Press, 1989.

[38] A. Rabl, "Comparison of solar concentrators," *Solar Energy,* vol. 18, no. 2, pp. 93-111, 1976.

[39] W. A. Baum, and J. D. Strong, "Basic optical considerations in the choice of a design for a solar furnace," *Solar Energy,* vol. 2, no. 3-4, pp. 37-45, 1958.

[40] V. Thakkar, A. Doshi, and A. Rana, "Performance Analysis Methodology for Parabolic Dish Solar Concentrators for Process Heating Using Thermic Fluid," *IOSR Journal of Mechanical and Civil Engineering (IOSR-JMCE),* vol. 12, no. 1, pp. 101-114, 2015.

[41] "Optics: How to Build a Beam Expander," September 15, 2017; http://assets.newport.com/webdocuments-en/images/how˙to˙build˙a˙beam˙expander˙5.pdf.

[42] TheEngineeringToolBox. "Emissivity Coefficients of Some Common Materials," 5 November 2017; https://www.engineeringtoolbox.com/emissivity-coefficients-d˙447.html.

[43] TheEngineeringToolBox. "Materials - Light Reflecting Factors," 5 November 2017; https://www.engineeringtoolbox.com/light-material-reflecting-factor-d˙1842.html.

[44] TheEngineeringToolBox. "Surface - Radiation Absorptivity," 5 November 2017; https://www.engineeringtoolbox.com/radiation-surface-absorptivity-d˙1805.html.